Relationship between the nonlinear ferroelectric and liquid crystal models for microtubules

M. V. Satarić[1] and J. A. Tuszyński[2]
[1]*Faculty of Technical Sciences, 21000 Novi Sad, Serbia, Yugoslavia*
[2]*Department of Physics, University of Alberta, Canada T6G 2J1*
(Received 27 December 2001; revised manuscript received 24 May 2002; published 6 January 2003)

Microtubules (MTs), which are the main components of the cytoskeleton, are important in a variety of cellular activities, but some physical properties underlying the most important features of their behavior are still lacking satisfactory explanation. One of the essential enigmas regarding the energy balance in MTs is the hydrolysis of the exchangable guanosine 5′-triphosphate bound to the β monomer of the molecule. The energy released in the hydrolysis process amounts to 6.25×10^{-20} J and has been the subject of many attempts to answer the questions of its utilization. Earlier, we put forward a hypothesis that this energy can cause a local conformational distortion of the dimer. This distortion should have nonlinear character and could lead to the formation of a traveling kink soliton. In this paper we use the formalism of the liquid crystal theory to consider the nonlinear dynamics of MTs. We demonstrate that this new model is formally equivalent to our earlier ferroelectric model which was widely exploited in an attempt to elucidate some important dynamical activities in MTs. We also study the stability of kink solitons against small perturbations and their unusual mutual interactions as well as the interactions with structural inhomogenities of MTs. Our new approach based on liquid crystal properties of microtubules has been recently corroborated by new insights gained from the electrostatic properties of tubulin and microtubules.

DOI: 10.1103/PhysRevE.67.011901 PACS number(s): 87.14.Ee, 87.15.−v, 87.16.−b

I. INTRODUCTION

Microtubules (MTs) are long and rigid tubular polymers. They assemble from tubulin, a protein found in eukaryotic cells, which ''crystallizes'' to form a helical lattice. Microtubules form an important part of the cellular scaffold and provide a network of ''rails'' for active intracellular transport. They also play a crucial role during cell division, forming a dynamic structure that spatially separates duplicated chromosomes.

Eighteen years ago, Mitchison and Kirschner [1,2] discovered that the polymerization of MTs from tubulin is a very interesting process in which an MT can repeatedly, and apparently at random, switch between persistent states of assembly and disassembly in a constant concentration of tubulin. This behavior is observed both *in vivo* and *in vitro* and is referred to as dynamical instability. This switching between growing and shrinking states at one concentration is unusual for a polymer. The energy required to do this is provided by hydrolysis of guanosine triphosphate (GTP), a nucleotide bound to assembling monomers. A reasonable possibility proposed by Mitchison and Kirschner is that these transitions occur as a consequence of competition between assembly and GTP hydrolysis. A growing MT assembles by the addition of GTP tubulin, which is later converted to guanosine diphosphate (GDP) tubulin. In that scenario, a growing MT has a stabilizing cap of GTP bound tubulins at the ends. If hydrolysis overtakes the addition of new GTP tubulins, the cap is gone and the MT end undergoes a change to the shrinking state, a so-called catastrophe. Conformational changes of tubulin or a structural change of the MT are other candidates for the explanation of dynamical instability [3]. In this paper, we propose a mechanism that unifies both of the aforementioned mechanisms in a single plausible approach. The recently discovered role of MTs in the communication between the extracellular matrix and the cell nucleus [4,5] provides additional motivation to study the biophysical properties of these protein filaments.

Several groups of researchers have developed models of energy trapping and propagation along a microtubular protofilament. Chou *et al.* [6] showed that kinks and pulses excited by the energy freed in the GTP hydrolysis can propagate along MTs due to elastic coupling between tubulin dimers. Another model of solitary wave formation was proposed by Satarić *et al.* [7], and further developed by Trpišóva and Tuszyński [8]. The working assumption in that model is that tubulin dimers possess dipole moments which are spontaneously ordered at physiological temperature. Consequently, solitary waves carrying the free portion of hydrolysis energy correspond to kink-type domain walls connecting two regions of the protofilaments with opposite electric polarizations.

In this paper we approach the problem of internal degrees of freedom in microtubules from a different view point by considering the microtuble in terms of a smectic ferroelectric liquid crystal system. Many components of living cells [9] such as cell membranes, DNA in chromosomes, proteins in muscles and in connective tissues (collagens) exhibit liquid crystal properties. Microtubules may similarly fall into the category of liquid crystals on at least two counts. First, the constituents of a nerve axon cell membrane are lipid molecules with chiral structure provided by lipid polar heads and tails, similarly to the shape of a polar tubulin dimer, shown in Fig. 1. Moverover, these lipid molecules mostly consist of α helices and β sheets and their longest dimension is about 4 nm which is comparable to tubulin. The second point is that Das and Schwarz [10] showed that cell membranes, especially of the nerve axon, could be considered in the framework of the theory of liquid crystals. Axons's symmetry is cylindrical and so is the symmetry of a microtubule.

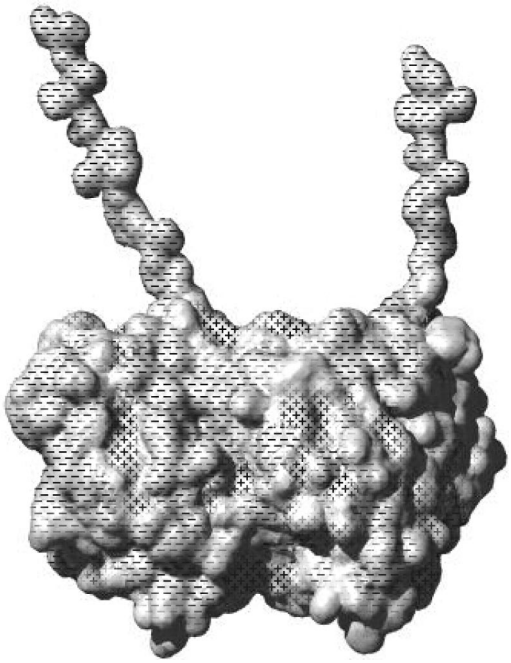

FIG. 1. A map of the electric charge distribution on the surface of a tubulin dimer with *C*-termini tails present. Figure prepared using MOLMOL [14].

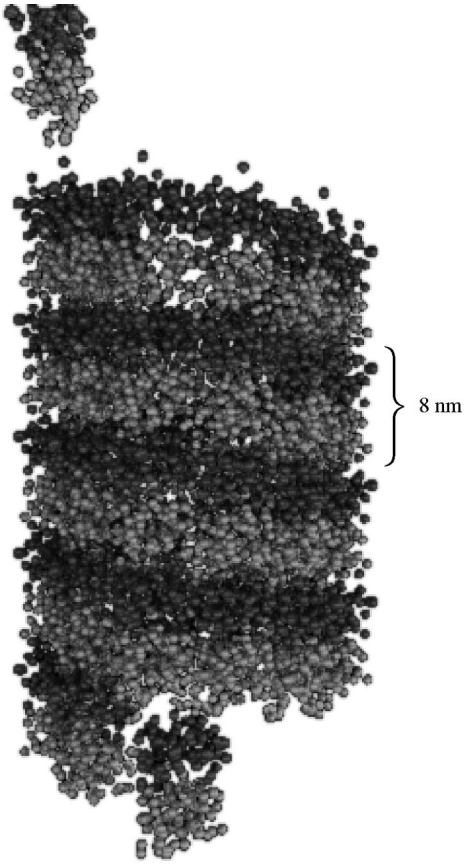

FIG. 2. A schematic drawing of an MT that consists of 13 protofilaments. The tubulin dimers are arranged in a helical manner (following Trpišóva and Tuszyński [8]).

This idea is further motivated by recent molecular dynamics simulations preformed by Tuszyński and co-workers [11]. These authors used the atomic resolution structure of tubulin from the protein data bank [12], and determined the electronic charge and dipole moment of tubulin and hence of an MT. Each tubulin monomer is comprised of approximately 450 amino acids and has about 7000 atoms. Its structure is very compact but can be divided into three functional domains; an amino-terminal domain constituting the nucleotide binding region (binding GTP or GDP), an intermediate domain containing the taxol-binding site, and a carboxy-terminal domain (*C* terminus) (see Fig. 1). This tail of the molecule has already been described biochemically by Sackett [13]. This chiral shape of the tubulin dimer, together with its electronic charge distribution treating the MT crystal as a supersmectic ferroelectric phase is suitable for modeling in terms of nonlinear dynamics.

The paper is organized as follows. Section II briefly reviews the earlier approach based on ferroelectric features of MTs leading to a nonlinear model giving rise to the existence of topological kink excitations. Section III introduces the liquid crystal framework based on the fact that the latest computational insights reveal that tubulin's chirality and dipole charge distribution fully justify such an approach. Section IV presents solutions of the nonlinear equation of motion and a discussion of their stability while the details of the stability analysis are relegated to the Appendix. Section V discussed the possible relationship between kink dynamics and dynamic instability in the context of the lateral cap model and conformational chages of tubulin.

II. AN OVERVIEW OF THE FERROELECTRIC MODEL OF MTs

The idea that MTs are ferroelectric was established on the basis of experimental evidence revealing that MTs exhibit pyroelectric and piezoelectric properties that arise as a result of elementary dipole moments carried by their subunit dimers [15].

Microtubules are hollow cylinders with a 25 nm outer and a 15 nm inner diameter (see Fig. 2). Each tubulin molecule is composed of two highly homologous monomers called α tubulin and β tubulin. The length of each dimer is approximately 8 nm, the width 5 nm, and the thickness also 5 nm. These dimers assemble themselves into protofilaments which typically number 13 although cylinders with 14 or even more protofilaments are routinely detected in experiments done *in vitro*. In the ferroelectric model proposed by Satarić *et al.* [7], the energy of an assembly of dipoles placed at discrete sites in a MT protofilament that consists of N tubulin dimers is represented by the following lattice Hamiltonian:

$$H=\sum_{n=1}^{N}\left[\frac{1}{2}M\left(\frac{du_n}{dt}\right)^2+\frac{1}{2}K(u_{n+1}-u_n)^2 - \left(\frac{\alpha_2}{2}u_n^2-\frac{\alpha_4}{4}u_n^4\right)-cu_n\right]. \tag{2.1}$$

In the equation above, the variable u_n represents the projection on the protofilament axis of the elastic displacement of the tubulin molecule corresponding to a different conformation. Describing the dynamics of the tubulin dimers in terms of only one of the variables (elastic degree of freedom) assumes that the other internal variable, i.e., the dipole moment behaves in the same way as u_n, in effect postulating that both variables are strongly coupled. Terms in Eq. (2.1) have the following interpretation: $\frac{1}{2}M(du_n/dt)^2$ is the kinetic energy of the tubulin molecule of mass M, $\frac{1}{2}K(u_{n+1}-u_n)^2$ represents the elastic energy that originates from the restoring elastic forces acting between two neighboring dimers. The quartic double well potential energy $V(u_n) = -(\alpha_2/2)u_n^2+(\alpha_4/4)u_n^4$ approximates the average effect of the surrounding dimers on the dimer at site n. The last term $: -cu_n$ in Eq. (2.1) accounts for the effect of an electric field to which the chain of dipoles in the protofilament can be exposed either within the cell or applied externally. The net electric field E at site n of the protofilament produces the potential energy $V_E=-cu_n=-q_{eff}Eu_n$, where q_{eff} is the effective charge of the nth tubulin dimer.

Furthermore, cellular MTs are embedded in cytosol, which is an electrolytic solution that interacts with the MTs both via electric forces and by providing a viscous medium which damps the displacements of tubulin dimers. This later effect can be modeled by including a frictional force in the equation of motion, where γ_D is the damping coefficient

$$F_v=\gamma_D\frac{\partial u_n}{\partial t}. \tag{2.2}$$

The Hamiltonian, Eq. (2.1), and the above force lead, in the continuum approximation, to the following equation of motion for the displacement field $u(x,t)$ of the dimer

$$M\frac{\partial^2 u(x,t)}{\partial t^2}-K\ell_0^2\frac{\partial^2 u(x,t)}{\partial x^2}-\alpha_2 u(x,t)+\alpha_4 u^3(x,t)+\gamma_D\frac{\partial u(x,t)}{\partial t}-q_{eff}E(x)=0. \tag{2.3}$$

Here, $\ell_0=8\times10^{-9}$ m is the equilibrium distance between the centers of mass of two neighboring tubulin dimers. The molecular weight of each tubulin monomer is 55 kDa so the dimer mass is $M=1.83\times10^{-22}$ kg. Note that inclusion of a random force, as dictated by general fluctuation dissipation arguments, has been attempted before [16], and it had a major effect on the kink's motion that was interpreted as slowing down the average propagation velocity.

An analytic kink-type solution of the above equation of motion, Eq. (2.3), was found in the form

$$u(\tau)=u_2+\frac{u_1-u_2}{1+\exp\left(\dfrac{u_1-u_2}{2}\tau\right)}, \tag{2.4}$$

where u_1 and u_2 are the real roots of the cubic polynomial in Eq. (2.3), and $\tau=x-vt$ represents the coordinate moving with the speed v (the propagation speed of the kink). As a result of the rather crude estimates for α_2 and α_4 given in Satarić *et al.* [7], it was determined that for a sufficiently small applied electric field E, the velocity of kink propagation v is proportional to the electric field strength E and it ranges from 10^{-2} m/s for $E\approx2\times10^5$ V/m to 10^{-4} m/s for $E=10^2$ V/m. These numbers appear to be on the high side of the known MT-associated processes (assembly and disassembly speeds or motor protein velocities), but may be relevant for coupled ionic waves or signaling modes that may accompany MT internal dynamics.

III. THE LIQUID CRYSTAL FRAMEWORK FOR MT DYNAMICS

Recently, Sirenko *et al.* [17] considered the MT as a thin elastic cylinder and calculated the attendant elastic vibrations whose maximum frequencies were found to be on the order of 10 GHz. They calculated the sound velocity along MTs and found it to be approximately $v_0\approx600$ m/s. The approach adopted does not depend on any specific features of the constituent dimers since it is strictly within a continuum model. This approach cannot provide answers regarding assembly and disassembly processes in MTs. We are convinced that a more fruitful approach is to incorporate the important intrinsic piezoelectric properties of MTs due to the presence of significant dipole moments of tubulin dimers already mentioned in Sec. I.

We now embark on the new approach to model MT dynamics based on the theory of liquid crystals. Drawing a parallel with the commonly accepted model of the nerve axon membrane given by Singer and Nicolson [18], we consider an MT to be a two-dimensional smectic ferroelectric liquid crystal composed of protein dimers which are folded into a cylinder with its characteristic dimensions depicted in Figs. 3 and 4. Very recently Thomas *et al.* [19] inferred experimentally that molecular chirality is expressed via chiral molecular packing in the tubule phase leading directly to the formation of helically arranged cylinders. A comprehensive review of the effects of molecular chirality in the formation of complex macromolecular structures with characteristic length scales can be found in Selinger *et al.* [20]. Examples of such structures involve the folding of lipid bilayers into tubules not unlike those formed by tubulin. This fact can be used as an explanation of the dimer packing in the MT cylinders.

The detailed map of the electric charge distribution on the surface of the tubulin dimer presented in Ref. [11] is shown in Fig. 1. It is clear that the C termini which extend outward carry significant electric charge. At neutral pH, the negative

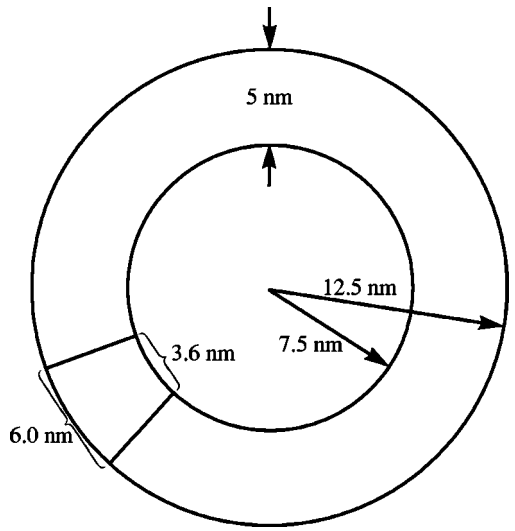

FIG. 3. The characteristic dimensions of an MT cylinder and the dimensions of wedgelike dimers built into the cylinder.

charge on each *C* terminus causes it to remain extended due to the electrostatic repulsion within the tail. A further experimental argument of significance to the model is that the dimers in MTs are highly deformable and undergo large amplitude conformational displacements. For example, when GTP hydrolysis occurs, the length of the tubulin dimer is reduced from 8.3 to 8.0 nm or by about 4%. This is far beyond thermal fluctuations and it requires the presence of an essentially nonlinear dynamics for its explanation.

It is also apparent that due to the strong curvature of an MT cylinder, the inner parts of dimers are compressed while the outer ones are stretched by a remarkable amount of tension (see Fig. 4). This situation provides the necessary conditions for a significant piezoelectric effect due to a redistribution of excess negative charges thus enhancing the transverse polarization in addition to the existing longitudinal one [7,8]. In Fig. 5 the usual ferroelectric liquid crystal geometry is presented for clarification. The dimer's director $\vec{n}$ is tilted from the layer's normal by an angle θ. The resultant electric polarization $\vec{p}=\vec{p}_t+\vec{p}_\ell$ is along the direction defined by $\vec{n}\times\hat{j}$ where $\hat{j}$ is a unit vector along the *y* axis (see Fig. 5). The vector $\vec{c}$ shown in Fig. 5 represents the *c* director which is the projection of $\vec{n}$ director laying in the smectic *x*-*y* plane with the angle φ with respect to the *x* axis. Introducing the piezoelectric coefficient μ_p we write the density of polarization energy in the following form:

$$W_{pol}=\frac{p_t^2}{2\chi_t}+\frac{p_\ell^2}{2\chi_\ell}-Ep_\ell-\mu_p p_t\theta, \tag{3.1}$$

where the corresponding longitudinal and transversal dielectric susceptibilities are denoted as χ_ℓ and χ_t, while the intrinsic electric field *E* [7,8] acts in the direction along the MT cylinder. The field $\vec{E}$ is assumed to be parallel to the *x* axis, along the protofilament, so that the corresponding electric interaction energy with the polarization $\vec{p}$ is $\vec{E}\cdot\vec{p}_\ell$, but for small angles this can be approximated by Ep_ℓ as in Eq. (3.1).

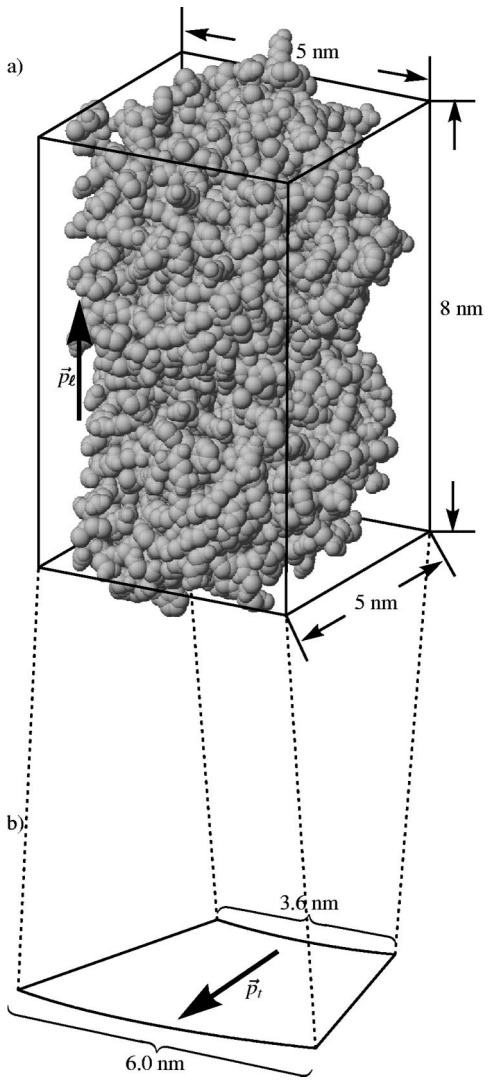

FIG. 4. (a) Free dimer with londitudinal dipole moment $\vec{p}_\ell$. (b) The dimensions of a deformed dimer and transverse dipole moment $\vec{p}_t$.

The phenomenological constant μ_p could be expressed in terms of model parameters as: (a) the anisotropy of molecular polarizability, (b) the angle between the steric dipole vector and the electric dipole of the same dimer which is the measure of chirality, (c) the length and average diameter of the dimer, and (d) the number density of dimers in a cylinder.

Following Carlsson *et al.* [21,22], the cylindrical smectic thin-layer elastic energy is expressed as follows:

$$W_{layer}=\frac{1}{2r^2}(A_{12}\sin^4\varphi+A_{21}\cos^4\varphi-2A_{11}\sin^2\varphi\cos^2\varphi), \tag{3.2}$$

with φ being the azimuthal angle of projection of the director vector $\vec{c}$ (see Fig. 5), while A_{12}, A_{21}, and A_{11}, are elastic coefficients. For clarification of the notation used in Fig. 5 please note that when $\theta=0$, $\vec{p}_\ell$ is parallel to the *x* axis and p_t to the *z* axis. When $\vec{n}$ is tilted at a small angle θ, so is $\vec{p}_\ell$

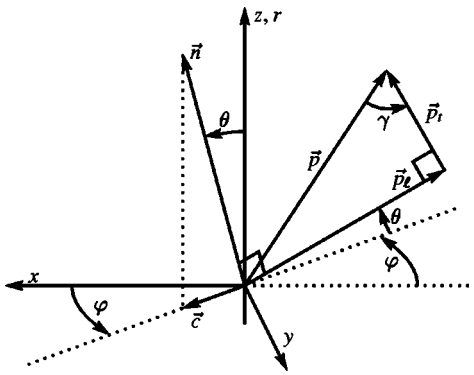

FIG. 5. The ferroelectric smectic C* liquid crystal geometry.

so that its projection on the x axis can be approximated by $p_t \sin\theta \approx p_t\theta$. The presence of the transverse component p_t is related to the existance of a charged *C*-termini feature in tubulin (see Fig. 5). Due to larger values of this tilt angle, the elastic coefficients can be expanded in powers of the tilt angle θ,

$$A_{12}=K_{11}+L_{12}\theta^2+M_{12}\theta^4,$$

$$A_{21}=K_{11}+L_{21}\theta^2+M_{21}\theta^4, \tag{3.3}$$

$$A_{11}=-K_{11}+L_{11}\theta^2+M_{11}\theta^4.$$

Here, K_{11} is the smectic C* splay elastic modulus. In the above expansions only even powers of θ are included because the energy functional must not change its value upon the inversion $\theta \rightarrow -\theta$. In view of Eq. (3.3) the elastic energy Eq. (3.2) now reads

$$W_{layer}=\frac{K_{11}}{2r}+\frac{1}{2r}\{[(L_{12}+L_{11})\sin^4\varphi+(L_{21}+L_{11})\cos^4\varphi]\theta^2 + [(M_{12}+M_{11})\sin^4\varphi+(M_{21}+M_{11})\cos^4\varphi]\theta^4\}. \tag{3.4}$$

Looking for the stable configuration regarding the angle φ we now minimize the layer energy with respect to φ yielding

$$[(L_{12}+L_{11})\sin^2\varphi-(L_{21}+L_{11})\cos^2\varphi] + [(M_{12}+M_{11})\sin^2\varphi-(M_{21}+M_{11})\cos^4\varphi]\theta^2=0. \tag{3.5}$$

The form of energy in Eq. (3.4) implies that the stable configuration φ_0 of the c director will depend on the signs of L_{ij} and M_{ij} $(i,j=1,2)$. Let us suppose that the following reasonable conditions hold:

$$(L_{12}+L_{11})+(M_{12}+M_{11})\theta^2>0,$$

$$(L_{21}+L_{11})+(M_{21}+M_{11})\theta^2>0, \tag{3.6}$$

so that the stable angle φ_0 may be given by the following expression:

$$\varphi_0=\tan^{-1}\sqrt{\frac{(L_{21}+L_{11})+(M_{21}+M_{11})\theta^2}{(L_{12}+L_{11})+(M_{12}+M_{11})\theta^2}}. \tag{3.7}$$

Solving for $\sin^2\varphi$ and $\cos^2\varphi$ using the minimization condition, Eq. (3.4), and replacing in the expression, Eq. (3.4), for layer elastic energy, retaining the terms up to fourth order in θ, we obtain the following expression:

$$W_{layer}=\frac{1}{r^2}(A\theta^2+B\theta^4), \tag{3.8}$$

where the new renormalized elastic coefficients A and B arise as follows:

$$A=\frac{(L_{12}+L_{11})(L_{21}+L_{11})}{(L_{11}+L_{12}+L_{21})}, \tag{3.9}$$

$$B=\frac{(L_{12}+L_{11})(M_{21}+M_{11})+(L_{21}+L_{11})(M_{12}+M_{11})}{(2L_{11}+L_{12}+L_{21})} - \frac{(L_{12}+L_{11})(L_{21}+L_{11})(M_{12}+M_{21}+M_{11})}{(2L_{11}+L_{12}+L_{21})^2}.$$

Eventually we should take into consideration the density of the splay elastic energy and the torsional kinetic energy of the dimer in MTs cylinder:

$$W_{sp}+W_{kin}=\frac{K_{11}}{2}\left(\frac{\partial\theta}{\partial x}\right)^2+\frac{\mathfrak{I}}{2}\left(\frac{\partial\theta}{\partial t}\right)^2, \tag{3.10}$$

where $\mathfrak{I}$ stands for the dimer's rotational inertia divided by the volume of a single dimer (the specific rotational inertia). Taking into account the wedgelike shape of a dimer in an MT, we estimated $\mathfrak{I}=3.1\times10^{-15}$ kg/m. Collecting the terms, Eqs. (3.1), (3.8), and (3.10), and summing over the whole cylinder, we obtain the total free energy as follows (d is the thickness of the cylinder):

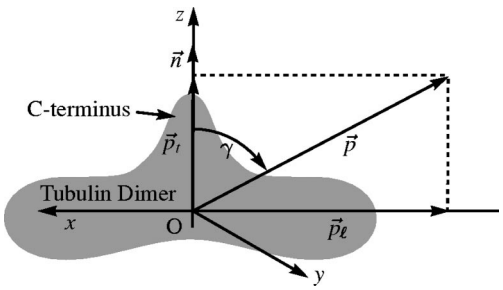

FIG. 6. The angle γ as a measure of chirality. A crude representation of a tubulin dimer is shown in gray.

$$F=2\pi\int_{R-d/2}^{R+d/2} r\,dr\int_{x_1}^{x_2} dx\left[\frac{K_{11}}{2}\left(\frac{\partial\theta}{\partial x}\right)^2+\frac{K_{11}}{2r^2}+\frac{A}{2r^2}\theta^2+\frac{B}{2r^2}\theta^4+\frac{\Im}{2}\left(\frac{\partial\theta}{\partial t}\right)^2+\frac{p_t^2}{2\chi_t}+\frac{p_\ell^2}{2\chi_\ell}-Ep_\ell-\mu_p p_t\theta\right]. \tag{3.11}$$

If we ignore the θ dependence on r due to the fact that the cylinder contains only one layer of dimers, we can integrate Eq. (3.11) with respect to r yielding

$$F=\int_{x_1}^{x_2} dx\left[\pi RK_{11}\left(\frac{\partial\theta}{\partial x}\right)^2+\pi K_{11}\ln\left(\frac{5}{3}\right)+\left[\pi A\ln\left(\frac{5}{3}\right)\right]\theta^2+\left[\pi B\ln\left(\frac{5}{3}\right)\right]\theta^4+2\pi Rd\left(\frac{p_t^2}{2\chi_t}+\frac{p_\ell^2}{2\chi_\ell}-Ep_\ell-\mu_p p_t\theta\right)\right]. \tag{3.12}$$

We now rely on Fig. 6 for illustration and write down the obvious trigonometric relations $p_\ell=p\sin\gamma$ and $p_t=p\cos\gamma$. The angle γ is considered to be a material constant at a given temperature and at a given pH of the solvent, and its value could be determined experimentally by performing measurements of both p_ℓ and p_t. It is a measure of the ratio between radial and longitudinal charge asymmetry within dimers caused by the curvature of an MT and the effects due to the changes on the *C* termini.

The free energy, Eq. (3.12), can now be minimized with respect to p, by finding $(\partial F/\partial p)=0$. Consequently one obtains

$$p=[E\sin\gamma+(\mu_p\cos\gamma)\theta]\Lambda(\gamma), \tag{3.13}$$

where $\Lambda(\gamma)$ stands for the expression $[(\sin^2\gamma/\chi_\ell)+(\cos^2\gamma/\chi_t)]^{-1}$. We infer that even if the external electric field is absent the resultant dipole electric moment of the dimer, Eq. (3.13), varies linearly with the tilt angle θ. Inserting p from Eq. (3.13) into Eq. (3.12) the free energy now reads

$$F=\int_{x_1}^{x_2} dx\left\{\pi K_b\left(\frac{\partial\theta}{\partial x}\right)^2+\frac{Rd\Im}{2}\left(\frac{\partial\theta}{\partial t}\right)^2+\frac{\pi K_b}{R}\ln\left(\frac{5}{3}\right)+\left[\frac{\pi Ad}{R}\ln\left(\frac{5}{3}\right)\right]\theta^2+\left(\frac{\pi Bd}{R}\ln\left(\frac{5}{3}\right)\right)\theta^4\right\}-[\pi Rd\Lambda(\gamma)\mu_p E\sin(2\gamma)]\theta-\pi Rd\Lambda(\gamma)E^2\sin^2(\gamma), \tag{3.14}$$

where $K_b=RK_{11}$. Here, we recognize the existence of a direct coupling of the external electric field to the mechanical deformation θ through the term proportional to $E\theta$ (the term before last). This coupling is maximal when $\gamma=(\pi/4)$.

If the dimers were nonchiral, i.e., for the piezoelectric transversal effect being zero, this term would have been zero and under such conditions there cannot be either solitary polarization waves or electrically induced propagation of the mechanical tilt field. Therefore, chirality induced by packing deformations of dimers is of essential importance for the results in this model. We already mentioned discussing Eq. (2.2) that the dimer's dynamics in MTs must account for the viscoelasticity so that the dynamical deformations are damped and subjected to increasing elastic forces. This frictional force now can be written in the form

$$F_v=-\Gamma\frac{\partial\theta}{\partial t}, \tag{3.15}$$

where $\Gamma=\ell_0\gamma_D$, ℓ_0, and γ_D were introduced in Sec. I. We are now able to develop an equation of motion for the tilt angle θ using Eq. (3.14) and Eq. (3.15). It simply reads

$$\pi K_b\frac{\partial^2\theta}{\partial x^2}-\pi Rd\Im\frac{\partial^2\theta}{\partial t^2}-\Gamma\frac{\partial\theta}{\partial t}-b\theta^3+a\theta+\tilde{c}=0, \tag{3.16}$$

where we used the following abbreviations

$$b=4\ln\left(\frac{5}{3}\right)\frac{\pi Bd}{R}, \tag{3.17}$$

$$a=2\ln\left(\frac{5}{3}\right)\frac{\pi Ad}{R}-2\pi Rd\Lambda(\gamma)\mu_p^2\cos^2\gamma, \tag{3.18}$$

and

$$\tilde{c}=\pi Rd\Lambda(\gamma)\sin(2\gamma)\mu_p E=\tilde{q}_{eff}E, \tag{3.19}$$

where $\tilde{q}_{eff}=\pi Rd\Lambda(\gamma)\sin(2\gamma)\mu_p$ represents the effective electric charge of a dimer in the context of the new model. We draw the reader's attention to the fact that the mathematical form of Eq. (3.16) coincides with Eq. (2.3) in the ferroelectric model of MT dynamics, Ref. [7]. However, here the anharmonic force $a\theta-b\theta^3$ originates from the double well potential reflecting the interaction between a tilting dimer and the surrounding dimers through the elastic coupling of the piezoelectric effect. The above potential actually stems from the expansion of the elastic energy coefficients that includes larger values of the tilt angle θ. It should be stressed

that polarization effects do not affect the nonlinear term governed by the parameter b. It is reasonable to expect that the inequality $b>0$ always holds. On the other hand, the parameter a exhibits a much richer dependence on both the elastic and polarization effects. Thus, the competition and interplay between the elastic and dielectric forces could even lead to a change of sign of the parameter a due to the change of temperature and/or or the strength of the applied electric field corresponding to the phase transition exhaustively discussed within the ferroelectric model in Trpišóva and Tuszyński [8]. The correlation length $\lambda=(\pi K_b/a)$ increases when the elastic and polarizational forces approach a balance.

IV. SOLUTIONS OF THE EQUATIONS OF MOTION AND THEIR STABILITY

We can now apply the procedure of finding solutions of this class of equations and then discuss the stability of the obtained solutions against small perturbations paying close attention to some recently discovered peculiar behavior of such nonlinear modes. In the case of a constant applied electric field, Eq. (3.16) can be solved analytically. In order to find a solution in the form of a traveling wave that moves at a constant velocity, a dimensionless moving coordinate $\xi=f(x-vt)$ is introduced as follows:

$$\xi=\sqrt{\frac{a}{\pi Rd\mathfrak{I}(v_0^2-v^2)}}(x-vt)=\kappa(x-vt), \tag{4.1}$$

where v_0 stands for the sound velocity in MTs. Using scaled variables $\eta(\xi)=\theta_0^{-1}\theta(\xi)$ and $\theta_0=\sqrt{a/b}$ and the traveling wave form of the solution, Eq. (4.1), one obtains the ordinary differential equation

$$\frac{d^2\eta}{d\xi^2}+\beta\frac{d\eta}{d\xi}+\eta-\eta^3+\varepsilon=0, \tag{4.2}$$

where the coefficients are defined as

$$\beta=\frac{\Gamma Rv}{\sqrt{\pi Rd\mathfrak{I}(v_0^2-v^2)}};\quad \varepsilon=\frac{\tilde{c}}{a}\sqrt{\frac{b}{a}}. \tag{4.3}$$

The traveling kink wave solution of Eq. (4.2) was first presented in Ref. [23], so we dispense with mathematical details giving only the final result,

$$\eta(\xi)=\eta_2+\frac{\eta_1-\eta_2}{1+\exp\left(\dfrac{\eta_1-\eta_2}{\sqrt{2}}\xi\right)}, \tag{4.4}$$

where $\eta_1=(2/\sqrt{3})\cos[\frac{1}{3}\cos^{-1}(\delta)]$ and $\eta_2=(2/\sqrt{3})\cos[2\pi/3+\frac{1}{3}\cos^{-1}(\delta)]$, where

$$\delta=\frac{3\sqrt{3}}{2},\quad \varepsilon=\frac{3\sqrt{3}\pi Rd\Lambda(\gamma)\sin(2\gamma)\mu_pE\sqrt{\dfrac{4\pi Bd}{R}\ln\left(\dfrac{5}{3}\right)}}{\left[\dfrac{4\pi Ad}{R}\ln\left(\dfrac{5}{3}\right)-4\pi Rd\Lambda(\gamma)\mu_p^2\cos\gamma\right]^{3/2}}. \tag{4.5}$$

The maximum value of the intrinsic electric field expected in MTs is calculated in Ref. [8] and yields $E_{max}=2.62\times10^6$ V/m. While not all the parameters contained in Eq. (4.5), are even approximately known, we could make an assumption that, similarly as in Ref. [7], the condition $\delta\ll1$ holds again. In that respect $\eta_1-\eta_2$ is positive and the kink tilt is arranged between the two states $\eta=\eta_1$ when $\xi\to-\infty$ and $\eta=\eta_2$ when $\xi\to+\infty$, traveling to the right. Since the argument δ is very small for every expected value of the electric field along an MT, η_1, and η_2 can be expanded around zero up to only the first order in δ, so the kink has a greatly simplified expression

$$\theta(\xi)=\sqrt{\frac{a}{b}}\left(-1+\frac{\delta}{\sqrt{27}}+\frac{2}{1+\exp(\sqrt{2}\xi)}\right). \tag{4.6}$$

Under the above set of conditions and using the expansion with respect to δ we obtain the equation for the kink's propagation velocity as follows:

$$v=\frac{3v_0}{\Gamma Ra}\sqrt{\frac{\mathfrak{I}Rbd}{2}}q_{eff}E. \tag{4.7}$$

This is the so-called terminal velocity for the given constant field E. Equation (4.7) shows how the velocity of kinks depends on the model parameters. The impact of polarization effects is included through the coefficients a and q_{eff}, while elasticity has a less pronounced effect as it only figures in $\sqrt{b}$. The role of viscosity is, in accordance with our expectations, to damp the motion. It could be safely inferred that a linear response of the kink velocity to the electric field can play the role as an important control mechanism for a host of cellular activities.

It is worth noting that the solution presented here was initially developed as a mechanism for structural phase transitions in crystals [24]. We conjecture that this mechanism of the kink drift could pertain to MTs in neural cells where they are very stable and it is believed that they play an important role in the organization and streamlining of the persistant flow of cellular components required for the leading edge activity. It is reasonable to assume that the electric field driven by the nerve cell's action potential affects MTs carrying kinks along them in the direction of their propagation.

In the Appendix, on the basis of kink stability analysis, we prove that in the absence of electric fields kinks exhibit random motion due to the action of small perturbations. The translational length of the kink's random displacement is given by the expression

$$L=C_2bv_0\sqrt{\frac{6\pi Rd\mathfrak{I}}{4a^3}}, \tag{4.8}$$

where C_2 is a constant. This means that the nonlinearity parameter b sustains the effect. Thus the random motion of kinks themselves or in combination with the drift motion regulated by electric fields could lead to numerous collisions between kinks presumably populated by the acts of ATP (adenosine triphosphate) hydrolysis as argued in Refs. [7,8].

Finally, we stress here that over the past decade much attention was paid to the discrete Klein-Gordon system especially applied to the chains of biomolecules. Our Eq. (3.16) pertains to the same class of equations if we take $\pi K_b(\theta_n - \theta_{n-1})^2$ instead of $\pi K_b(\partial\theta/\partial x)^2$ in the functional in Eq. (3.14). The numerical investigations performed by Dauxios *et al.* [25], Bang and Peyrard [26], Forinash *et al.* [27], Peyrard [28] unambiguously show that nonlinear excitations in such discrete systems exhibit some peculiar nonsolitonlike features. Namely, while ''pure'' solitons in the event of mutual scattering pass through each other without a change of energy or shape, the discrete nonlinear excitations in mutual interactions coalesce so the larger excitations grow at the expense of smaller ones. This process saturates when the solitons that get narrower as they collect more energy, are so narrow that they become trapped by discreteness of the lattice and are no longer able to move in the lattice.

Recently very precise experiments of Chretien *et al.* [29], Janosi *et al.* [30] revealed that microtubule cylinders may undergo remarkable bendings which indicates a sizeable stretching and compression of tubulin subunits along the protofilaments. Thus, we firmly believe that the formation of localized modes caused by ATP hydrolysis seems likely to occur, especially because biological molecules combine two possible sources of localization; nonlinearity and discreteness. Such local modes could have a dramatic effect if these anomalously large fluctuations (tilting rotation in the case of MTs) are at the origin of chemical reactions. In the case of microtubules an effect of this type could easily cause the onset of a disassembly process.

V. CONCLUSION AND DISCUSSION

Starting from new convincing arguments in Ref. [11] revealing the chirality and piezoelectric features of the tubulin molecule, as well as drawing a parallel with the geometry of the neuronal cell membrane [10], we adopted the framework of the ferroelectric liquid crystal theory [21,22] to describe nonlinear dynamics of MTs. We also relied here on the findings of Caplow *et al.* [31] that much of the free energy of GTP hydrolysis is coupled to the structural changes associated with dimer-dimer interactions leading to MT assembly. Similarly, Mandelkow *et al.* [32] observed that within an MT, a dimer that experiences hydrolysis of GTP is led to an energetically unfavorable (tense) large conformation which tends to relax the corresponding filament towards a coiled conformation. However, lateral bonds between filaments prevent such an effect and instead, neighboring dimers are also tilted by the energy released. Within our model this corresponds to the formation of a deformation defect. Its drift motion superposed with diffusive motion pushes it preferentially towards the positive end of an MT since the intrinsic electric field is directed from the plus to the minus end and the kink reorients the dipoles as it moves. Since the MT ends are exposed to the environment and less stablized by interfilament bonds than the MT interior, relaxation into the coiled configuration takes place most readily at the ends [29,30]. Therefore, the MT tips can be seen as the weakest points of the MT structure. It is not very likely, however, that thermal fluctuations could cause massive depolymerization at MT ends.

We assume that kinks produced by GTP hydrolysis inside the MT could reach the end and relax the tension through a detachement of many dimers from the tip. This would be especially relevant if the MT end consisted of dimers already burdened by tension due to GTP hydrolysis. The fact that kinks spend some time traveling towards an MT end produces a certain delay in the activation of disassembly with respect to the time of a kink's excitation. This delay depends on the kink's velocity and the distance traveled. However, if the considered MT end is protected by a so-called latteral cap of at least 10–20 dimers loaded by unhydrolyzed GTP, the tip structure is robust enough that an incoming kink cannot lead to a catastrophic event of rapid disassembly.

The following experimental obsevations can be cited in support of our hypothesis:

(a) If the tubulin is loaded with a nonhydrolyzable GTP analog instead of GTP, very stable MTs are polymerized [33]. There is no ''fuel'' for kink formation and there is no enough tension to cause a dynamical instability.

(b) On the other hand, the addition of Ca^{2+} ions in a solution of tubulin GTP leads to an increase in the rate of hydrolysis of GTP in the lateral cap and inside MTs, producing more kinks and increasing the rate of catastrophic disassembly events [34].

(c) Dhamodharam *et al.* [35] have shown that when the drug vinblastine is added to the caps of MTs in living cells, despite GTP hydrolysis along the MTs the diassembly of MTs is stopped since kinks may not destabilize the thus strengthened ends. This promotes vinblastine as an antitumor drug that suppresses mitotic spindle formation by arresting MT dynamics.

We now comment on the role on microtubule associated proteins (MAPs) in the process of stabilizing MTs. A higher stability of MTs in neurons can be explained by a higher content of MAPs in these cells. Particularly efficient in that respect is the τ (tau) protein. Even at low concentrations (0.1–0.2 M), τ protein dramatically reduces the catastrophe frequency of MTs. If τ is phosphorylated by MAP2 kinase, which decreases the affinity of τ for MT binding tenfold, the role of τ protein in suppressing MT dynamics decreases proportionally.

We conjecture that the attachment of MAPs to MTs involves the generation of inhomogeneities in MTs via local potential deformations present along the path of a moving kink. This was studied numerically by Trpišóva and Tuszyński [8], where it was shown that for large enough potential wells, kink motion can be significantly slowed down or stopped altogether. This would prevent kinks from reaching the MT ends and from releasing the energy stored in them. This is consistent with the fact that increasing the number of MAPs enhances the stability of MTs.

The above discussion was intended to emphasize the practical importance of our analytical solution in Eq. (4.6) and Eq. (4.7) obtained within the continuum approximation of the model in Eq. (3.16). Future investigations based on a discrete model similar to those presented in Ref. [28] should reveal new features of kink dynamics and a better comparison with experimental data.

Finally, we wish to mention the connection of our work with the findings of Maniotis *et al.* [5]. This team of cell biologists has demonstrated that mammalian cells are densely ''hard-wired'' with force-carrying connections (MTs, actin filaments, intermediate filaments) that reach all the way from the membrane through the cytoskeleton to the cell nucleus. We conjecture that mechanical stress coupled with piezoelectric changes in MTs causes strong local conformations of dimers producing kinks which carry mechanical tension to the cell nucleus. This puts the cytoskeleton in a new light as a mechanism for signal transduction rather than just a mechanical scaffold. We expect that careful measurements of the dynamic structure factor using neutron scattering off solutions of dynamically unstable MTs should demonstrate kink dynamics and we encourage experimentalists to pursue such measurements. In the past, kink contributions to the neutron scattering cross section were calculated in the context of structural phase transitions [36]. Calculations of this mechanism's contribution to neutron scattering from microtubules are currently underway and should assist in future experiments.

ACKNOWLEDGMENTS

This research project was supported by grants from NSERC and MITACS-MMPD. Additional support was received from the Theoretical Physics Institute at the University of Alberta. The authors gratefully acknowledge the assistance of Mr. Eric Carpenter.

APPENDIX

If we start from the much studied case where Eq. (3.16) is taken without the influence of viscosity and electric fields, the remaining part of the equation reads

$$\pi R d \mathfrak{I} \frac{\partial^2 \theta}{\partial t^2} - a\,\theta + b\,\theta^3 - \pi R K_b \frac{\partial^2 \theta}{\partial x^2} = 0. \tag{A1}$$

The most important solution of Eq. (A1) is the domain wall excitation, which may be expressed as

$$\theta_{DW} = \theta_0 \tanh(\xi), \tag{A2}$$

where ξ is the same as in Eq. (4.1). We now check whether the solution, Eq. (4.6), of our nonlinear form, Eq. (3.16), is stable against small perturbations. To this end we assume the solution of the perturbed system, Eq. (3.16), to be in the form

$$\theta(x,t) = \theta_{DW}(x,t) + \Psi(x,t), \tag{A3}$$

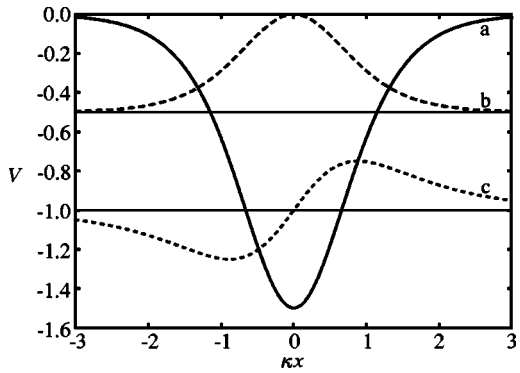

FIG. 7. (a) Plot of potential $-\frac{3}{2}\mathrm{sech}^2(\kappa x)$. (b) Plot of bound state $g_1(x) = A_1 \mathrm{sech}^2(\kappa x)$. (c) Plot of bound state $g_2(x) = A_2[\sinh(\kappa x)/\cosh^2(\kappa x)]$.

where $\Psi(x,t) \ll \theta_{DW}(x,t)$. In addition, we impose a condition that at time $t=0$, the domain wall is localized at $x=0$.

Thus the linearized equation of motion for the perturbation function $\Psi(x,t)$ according to Eq. (3.16) yields

$$2\pi R d \mathfrak{I} \frac{\partial^2 \Psi}{\partial t^2} + \Gamma \frac{\partial \Psi}{\partial t} + 2a[1 - \tfrac{3}{2}\mathrm{sech}^2(\xi)]\Psi - \pi R K_b \frac{\partial^2 \Psi}{\partial x^2} = -\tilde{c}. \tag{A4}$$

In order to solve this equation we first inspect a similar equation that is well known from quantum mechanics,

$$\left[2\pi R d \mathfrak{I} \frac{\partial^2}{\partial t^2} + 2a[1 - \tfrac{3}{2}\mathrm{sech}^2(\xi)] - \pi R K_b \frac{\partial^2}{\partial x^2}\right] g(x) = 0, \tag{A5}$$

separating the variables by the usual transformation, $g(x) = \exp(i\omega t) \cdot f(x)$, Eq. (A5) gives

$$\left[2\pi R d \mathfrak{I} \omega^2 + 2a[1 - \tfrac{3}{2}\mathrm{sech}^2(\xi)] - \pi R K_b \frac{\partial^2}{\partial x^2}\right] f(x) = 0. \tag{A6}$$

This is a Schrödinger-type equation with a potential of the form $-\mathrm{sech}^2(\xi)$. Figure 7 depicts the potential and the eigenfunctions of its two bound states.

The complete set of solutions to Eq. (A6) is given as follows:

$$g_1(x) = A_1 \mathrm{sech}^2(\kappa x), \quad \omega_1 = 0, \tag{A7}$$

$$g_2(x,t) = A_2 \exp(i\omega_2 t) \frac{\sinh(\kappa x)}{\cosh^2(\kappa x)}, \quad \omega_2 = 3\sqrt{\frac{a}{4\pi R d \mathfrak{I}}}, \tag{A8}$$

and the infinite set of continuum solutions given by

$$g_s(x,t) = A_s \exp(i\omega_s t) \exp(is\kappa x)[3\tanh^2(\kappa x) - (1+s^2) + 3is\tanh(\kappa x)], \tag{A9}$$

where $\omega_s=(4+s^2)\sqrt{(a/4\pi Rd\mathfrak{I})}$, $-\infty\leqslant s\leqslant+\infty$, and A_1, A_2, and A_s stand for the corresponding normalization constants. Since the auxiliary system considered here, Eq. (A6) possesses a complete set of eigenfunctions, Eqs. (A7), (A8), and (A9), we can expand the function $\Psi(x,t)$ that appears in Eq. (A4) with respect to this set as follows:

$$\Psi(x,t)=T_1(t)g_1(\kappa x)+T_2(t)g_2(\kappa x)+\int_{-\infty}^{+\infty}dsT_s(t)g_s(x,t). \tag{A10}$$

Substituting this expression into Eq. (A4) and using the orthogonality of the basis set we finally obtain

$$\frac{d^2T_j}{dt^2}+\left(\frac{\Gamma}{2\pi Rd\mathfrak{I}}+2i\omega_j\right)\frac{dT_j}{dt}+i\omega_j\left(\frac{\Gamma}{2\pi Rd\mathfrak{I}}\right)T_j=-\tilde{c}\exp(i\omega_j t)A_jf_j(\kappa x), \tag{A11}$$

for $j=1,2,3,\ldots$. The general solution of the homogeneous part of the above differential equation reads

$$T_j(t)=C_1\exp[-(\rho_a+\rho_b)t]+C_2\exp[-(\rho_a-\rho_b)t], \tag{A12}$$

where

$$\rho_a=i\omega_j+\frac{1}{2}\cdot\frac{\Gamma}{2\pi Rd\mathfrak{I}},\quad \rho_b=\frac{1}{2}\sqrt{\left(\frac{\Gamma}{2\pi Rd\mathfrak{I}}\right)^2-4\omega_j}. \tag{A13}$$

If $(\Gamma/2\pi Rd\mathfrak{I})^2>4\omega_j$ then both solutions in Eq. (A4) decay exponentially with time.

Specifically, for the first bound state where $\omega_1=0$ the real parts in Eq. (A13) cancel and $T_1(t)$ oscillates harmonically with time. In this case the solution of the homogenous part of Eq. (A12) is $\Psi_1=C_2$.

Returning to Eq. (A7) we obtain the corresponding perturbation function $\Psi(x,t)=C_2A_1\mathrm{sech}^2(\kappa x)$. Enforcing the normalization condition, $A_1^2\int_{-\infty}^{+\infty}dx\mathrm{sech}^4(\kappa x)=1$ and adding the particular solution of the inhomogenous equation, (A11),

$$\Psi_p=\frac{\tilde{c}A_j\exp(i\omega_j t)f_j(\kappa x)}{3\omega_j^2-2i\omega_j\left(\frac{\Gamma}{2\pi Rd\mathfrak{I}}\right)}, \tag{A14}$$

we express the perturbation function in the form

$$\Psi(x,t)=C_2bv_0\sqrt{\frac{6\pi Rd\mathfrak{I}}{4a^3}}\cdot\frac{d\theta_{DW}}{dx}+\frac{\tilde{c}A_j\exp(i\omega_j t)f_j(\kappa x)}{3\omega_j^2-2i\omega_j\left(\frac{\Gamma}{2\pi Rd\mathfrak{I}}\right)}, \tag{A15}$$

where we have used the identity $(d/dx)\tanh x=\mathrm{sech}^2x$ and Eq. (A2). Thus, the function describing the tilt angle θ in the presence of a perturbation has the form

$$[\theta(x,t)]_{t\to\infty}=\theta_{DW}+L\frac{d\theta_{DW}}{dx}=\theta_{DW}(x+L)+\frac{\tilde{c}A_j\exp(i\omega_j t)f_j(\kappa x)}{3\omega_j^2-2i\omega_j\left(\frac{\Gamma}{2\pi Rd\mathfrak{I}}\right)}, \tag{A16}$$

where the translational length of the kink's displacement has the value

$$L=C_2bv_0\sqrt{\frac{6\pi Rd\mathfrak{I}}{4a^3}}. \tag{A17}$$

The second term in Eq. (A16) is always limited so that this solution exhibits stability against external perturbations. The reader is referred to Currie *et al.* [37] for additional insights and initial presentation of the stability analysis presented here.

[1] T.J. Mitchison and M.V. Kirschner, Nature (London) **312**, 232 (1984).
[2] T.J. Mitchison and M.V. Kirschner, Nature (London) **312**, 237 (1984).
[3] M. Caplow, Curr. Opin. Cell Biol. **4**, 58 (1992).
[4] J. Glanz, Science **276**, 678 (1997).
[5] A.J. Maniotis, C.S. Chen, and D.E. Ingber, Proc. Natl. Acad. Sci. U.S.A. **94**, 849 (1997).
[6] K.C. Chou, C.T. Zhang, and G.M. Maggiora, Biopolymers **34**, 143 (1994).
[7] M.V. Satarić, J.A. Tuszyński, and R.B. Żakula, Phys. Rev. E **48**, 589 (1993).
[8] B. Trpišóva and J.A. Tuszyński, Phys. Rev. E **55**, 3288 (1997).
[9] M. Ho, *The Rainbow and the Worm: The Physics of Organisms* (World Scientific, Singapore, 1998).
[10] P. Das and W.H. Schwarz, Phys. Rev. E **51**, 3588 (1995).
[11] J.A. Tuszyński, J.A. Brown, E.J. Carpenter, E. Crawford, and M.L.A. Nip, in *Proceedings of the ESA-IEJ Joint Meeting, Evanston, 2002* (Laplacina Press, Morgan Hill, CA, 2002), p. 41.
[12] H.M. Berman, J. Westbrook, Z. Feng, G. Gilliland, T.N. Bhat, H. Weissig, I.N. Shindyalov, and P.E. Bourne, Nucleic Acids Res. **28**, 235 (2000).
[13] D.L. Sackett, *Subcellular Biochemistry, Proteins: Structure, Function and Engineering* (Plenum Press, New York, 1995), Vol. 24, p. 255.
[14] R. Koradi, M. Billeter, and K. Wüthrich, J. Mol. Graphics **14**, 51 (1996).
[15] H. Athenstaedt, Ann. N.Y. Acad. Sci. **238**, 68 (1974).

[16] H. Rosu, J.A. Tuszyński, and A. Gonzalez, Nuovo Cimento D **20**, 369 (1998).
[17] Y.M. Sirenko, M.A. Stroscio, and K.W. Kim, Phys. Rev. E **53**, 1003 (1996).
[18] S.J. Singer and G.L. Nicolson, Science **175**, 720 (1972).
[19] B.N. Thomas, C.M. Lindemann, and N.A. Clark, Phys. Rev. E **59**, 3040 (1999).
[20] J.V. Selinger, M.S. Spector, and J.M. Schnur, J. Phys. Chem. B **105**, 7157 (2001).
[21] T. Carlsson, I.W. Stewart, and F.M. Leslie, Liq. Cryst. **9**, 661 (1991).
[22] T. Carlsson, I.W. Stewart, and F.M. Leslie, Liq. Cryst. **11**, 49 (1992).
[23] E.W. Montroll, *Statistical Mechanics* (University of Chicago Press, Chicago, 1972).
[24] J.A. Krumhansl and J.R. Schrieffer, Phys. Rev. B **11**, 3535 (1975).
[25] T. Dauxois, M. Peyrard, and C.R. Willis, Phys. Rev. E **48**, 4768 (1993).
[26] O. Bang and M. Peyrard, Phys. Rev. E **53**, 4143 (1996).
[27] K. Forinash, T. Cretegny, and M. Peyrard, Phys. Rev. E **55**, 4740 (1997).
[28] M. Peyrard, Physica D **119**, 184 (1998).
[29] D. Chretien, H. Flyvbjerg, and S. Fuller, Eur. Biophys. J. **27**, 490 (1998).
[30] I.M. Janosi, D. Chretien, and H. Flyvbjerg, Eur. Biophys. J. **27**, 501 (1998).
[31] M.R. Caplow, L. Ruhlen, and J. Shanks, J. Cell Biol. **127**, 779 (1994).
[32] E. Mandelkow, E. Mandelkow, and R.A. Malligan, J. Cell Biol. **144**, 991 (1991).
[33] M.R. Mejillano, J.S. Barton, and R.H. Himes, Biochem. Biophys. Res. Commun. **166**, 653 (1990).
[34] E.T. O'Brien, E.D. Salmon, and H.P. Erickson, Cell Motil. Cytoskeleton **36**, 125 (1997).
[35] R. Dhamodharam, M.A. Jordan, D. Thrower, L. Wilson, and P. Wadsworth, Mol. Biol. Cell **6**, 1215 (1995).
[36] A.R. Bishop, J. Phys. A **14**, 1417 (1981).
[37] J.F. Currie, S. Sarker, A.R. Bishop, and S.E. Trullinger, Phys. Rev. A **20**, 2213 (1979).